

# UC Riverside

## UC Riverside Previously Published Works

### Title

Enhanced weathering strategies for stabilizing climate and averting ocean acidification

### Permalink

<https://escholarship.org/uc/item/3hw1h419>

### Journal

Nature Climate Change, 6(4)

### ISSN

1758-678X

### Authors

Taylor, Lyla L  
Quirk, Joe  
Thorley, Rachel MS  
[et al.](#)

### Publication Date

2016-04-01

### DOI

10.1038/nclimate2882

Peer reviewed

1 **Enhanced weathering strategies for stabilizing climate and averting**  
2 **ocean acidification**

3 Lyla L. Taylor<sup>1</sup>, Joe Quirk<sup>1</sup>, Rachel M.S. Thorley<sup>1</sup>, Pushker A. Kharecha<sup>2,3</sup>,  
4 James Hansen<sup>2</sup>, Andy Ridgwell<sup>4,5</sup>, Mark R. Lomas<sup>6</sup>, Steve A. Banwart<sup>7</sup>  
5 & David J. Beerling<sup>1\*</sup>

6 <sup>1</sup>Department of Animal and Plant Sciences, University of Sheffield, Sheffield S10 2TN, UK

7 <sup>2</sup>Earth Institute, Columbia University, 475 Riverside Drive, New York, 10027, USA

8 <sup>3</sup>Goddard Institute for Space Studies, NASA, 2880 Broadway, New York, 10025, USA

9 <sup>4</sup>Department of Geographical Sciences, University of Bristol, Bristol BS8 1SS, UK

10 <sup>5</sup>Department of Earth Sciences, University of California, Riverside CA, 92521, USA

11 <sup>6</sup>Department of Mathematics, University of Sheffield, Sheffield S10 2TN, UK

12 <sup>7</sup>Kroto Research Institute, North Campus, University of Sheffield, Sheffield S3 7HQ, UK

13

14 \*Email [d.j.beerling@sheffield.ac.uk](mailto:d.j.beerling@sheffield.ac.uk)

15 Chemical breakdown of rocks, ‘weathering’, is an important but very slow part of the  
16 carbon cycle that ultimately leads to CO<sub>2</sub> being locked-up in carbonates on the ocean  
17 floor. Artificial acceleration of this carbon sink via distribution of pulverized silicate  
18 rocks across terrestrial landscapes may help offset anthropogenic CO<sub>2</sub> emissions<sup>1-5</sup>. We  
19 show that idealized enhanced weathering scenarios over less than a third of tropical land  
20 could significantly drawdown atmospheric CO<sub>2</sub> and ameliorate ocean acidification by  
21 2100. Global carbon cycle modelling<sup>6-8</sup> driven by ensemble Representative  
22 Concentration Pathway (RCP) projections of 21<sup>st</sup> century climate change (RCP8.5,  
23 business-as-usual; RCP4.5, medium-level mitigation)<sup>9,10</sup>, indicates that enhanced  
24 weathering could lower atmospheric CO<sub>2</sub> by 30-300 ppm by 2100 depending mainly on  
25 silicate rock application rate (1 kg or 5 kg m<sup>-2</sup> yr<sup>-1</sup>) and composition. At the higher  
26 application rate, end-of-century ocean acidification is reversed under RCP4.5 and  
27 reduced by about two-thirds under RCP8.5. Additionally, surface ocean aragonite  
28 saturation state, a key control on coral calcification rates, is maintained above 3.5  
29 throughout the low latitudes, thereby helping maintain the viability of tropical coral reef  
30 ecosystems<sup>11-14</sup>. However, we highlight major issues of cost, social acceptability, and  
31 potential unanticipated consequences that will limit utilization and emphasize the need  
32 for urgent efforts to phase down fossil fuel emissions<sup>15</sup>.

33 In 1992, over 170 nations agreed to limit anthropogenic CO<sub>2</sub> emissions to avoid ‘dangerous’  
34 human-made climate change<sup>16</sup>, yet massive expansion of fossil fuel extractions, including  
35 shale gas and tar sands, is allowing emissions to grow<sup>17</sup>. Avoiding dangerous climate change  
36 may therefore require the controversial deployment of Carbon Dioxide Removal (CDR)  
37 schemes<sup>4,18</sup>, so called ‘negative emissions’ strategies whereby CO<sub>2</sub> is captured and removed  
38 from the atmosphere. The Fifth Assessment Report of the Intergovernmental Panel on  
39 Climate Change<sup>12</sup> and the U.S. National Research Council Report<sup>18</sup> both recognized enhanced  
40 terrestrial weathering of silicate rocks as an important but poorly constrained CDR approach.  
41 Currently, natural weathering of silicate and carbonate rocks consumes ~0.25 Pg C yr<sup>-1</sup> of  
42 atmospheric CO<sub>2</sub>, which is ~3% of fossil fuel emissions<sup>19</sup> (~9–10 Pg C yr<sup>-1</sup>). Artificially  
43 accelerating this land-based CO<sub>2</sub> sink involves the intentional application of pulverised  
44 silicate rocks to vegetated landscapes to markedly enhance CO<sub>2</sub> consumption<sup>1-5</sup>. However,  
45 assessments to date have excluded primary drivers of soil mineral weathering, especially  
46 terrestrial ecosystem processes and feedbacks from CO<sub>2</sub> and future climate change, limiting  
47 our understanding of its capacity to offset fossil fuel CO<sub>2</sub> emissions<sup>12</sup>.

48 Here we present spatially resolved analyses of enhanced weathering by terrestrial  
49 ecosystems as a macro-engineering CDR option based on idealized cases for distributing  
50 pulverised silicate rocks in the tropics using multi-model ensemble projections (Coupled  
51 Model Intercomparison Project, CMIP5) of 21<sup>st</sup> century climate change<sup>9,10</sup>. Our modelling  
52 framework includes climate-plant-soil linkages important for regulating mineral weathering  
53 by coupling a detailed weathering model with a dynamic global vegetation model and  
54 accounting for land surface hydrology, topography and lithology<sup>6,7</sup> (Methods). We assess  
55 effects of enhanced weathering on net CO<sub>2</sub> consumption and examine feedbacks on  
56 atmospheric CO<sub>2</sub> and ocean chemistry over the next century using a suite of five CMIP5  
57 general circulation model (GCM) simulations (1°lat. × 1°lon.)<sup>9,10</sup> for each of two  
58 Representative Concentration Pathway scenarios (RCPs): RCP8.5 (business-as-usual), and  
59 RCP4.5 (medium-level stabilization of emissions); postscripts (8.5 and 4.5) denote radiative  
60 forcing (W m<sup>-2</sup>) in year 2100 relative to year 1750 (Supplementary Information).  
61 Assessments are undertaken for various application rates of the igneous rocks dunite (>90%  
62 olivine, Mg<sub>2</sub>SiO<sub>4</sub>) (Ref. 3) and harzburgite (50–90% olivine), which are both commercially  
63 mined, and basalt for which major resources exist in terrestrial large igneous provinces  
64 (LIPs)<sup>20</sup> (Fig. 1). These rates fall within the range adopted in the early 1930s for rejuvenating  
65 European forest soils with basalt to encourage tree growth<sup>21</sup>.

66 Our simulations indicate that terrestrial weathering can be markedly increased by  
67 distributing pulverised silicate rocks throughout the tropics (30°N to 30°S), potentially  
68 consuming hundreds of petagrams ( $1 \times 10^{15}$  g) of CO<sub>2</sub> by 2100 (Fig. 1). Ensemble median  
69 CO<sub>2</sub> consumption by terrestrial weathering increases towards a maximum as the total rock  
70 applied increases, with olivine-rich dunite and harzburgite being about twice as effective as  
71 basalt for equivalent application rates (Fig. 1a–c). We present CO<sub>2</sub> consumption curves  
72 assuming mixing depths of 10 cm and 30 cm for each application rate; 10 cm is likely the  
73 minimum mixing depth given intense precipitation events, the distribution of macropores and  
74 bioturbation by invertebrates in tropical soils down to depths of 30–50 cm (Supplementary  
75 Information). In the model, CO<sub>2</sub> consumption by weathering increases when added rock  
76 grains mix deeper in the soil, particularly at the 5 kg m<sup>-2</sup> yr<sup>-1</sup> application rate, because mineral  
77 saturation, a chemical brake on weathering, occurs more slowly in a larger soil solution  
78 volume. Overall CO<sub>2</sub> consumption patterns for a particular RCP scenario show a consistently  
79 narrow range of variation across the five ensemble GCMs (Fig. 1d–f). For a given application  
80 rate, the magnitude of CO<sub>2</sub> consumption is similar for the business-as-usual (RCP8.5) and  
81 medium level mitigation (RCP4.5) scenarios (Fig. 1d–f), largely because the runoff for the two  
82 scenarios is similar (Supplementary Information).

83 Comparing cumulative end-of-century amounts of pulverised rock added to the tropics  
84 with estimated total resources indicates dunite has limited utility for long-term atmospheric  
85 CO<sub>2</sub> removal<sup>3</sup> (Fig. 1), whereas sufficient harzburgite and basalt resources exist for the  
86 application rates considered here (Fig. 1, Supplementary Information). The rock mass  
87 required can be reduced by restricting application to regional intense tropical weathering  
88 ‘hotspots’ (Fig. 1, Supplementary Information). Such optimization reduces the land area  
89 required by more than two-thirds, from 69 Mkm<sup>2</sup> to 20 Mkm<sup>2</sup>, and total rock mass by 70%,  
90 whilst still achieving ~80–89% of the effect (Fig. 1a–c, symbols). Hotspot land areas are  
91 primarily tropical forests except parts of Asia which are croplands. However, basalt can  
92 promote crop growth on highly weathered acidic tropical soils<sup>22,23</sup> by increasing soil  
93 alkalinity, cation exchange capacity and the availability of growth-limiting phosphorus, with  
94 associated reductions in Al and Mn toxicity<sup>23,24</sup>. Ample basalt resources exist within the  
95 major LIPs in the tropics (Ethiopian Traps, Deccan Traps and Paraná Traps) to support  
96 simulated application rates (Fig. 1) and these sources could exploit existing infrastructure for  
97 distribution. Meeting silicate rock demand would require large-scale mining operations, e.g.,

98 throughout the major tropical LIPs, with production rates exceeding those for coal and  
99 adverse consequences for local ecosystems.

100 As CO<sub>2</sub> is removed from the atmosphere by enhancement of the weathering carbon sink,  
101 the carbon cycle responds by redistributing carbon among surface reservoirs (atmosphere,  
102 ocean, soil, and land biosphere), with CO<sub>2</sub> out-gassing by the ocean in particular offsetting  
103 some of the artificial drawdown<sup>17</sup>. There is, consequently, a ‘rebound’ effect whereby each  
104 extra mole of CO<sub>2</sub> consumed does not translate into the removal of a mole of atmospheric  
105 CO<sub>2</sub> over time. We therefore estimate the effects of our CO<sub>2</sub> consumption fluxes on the  
106 RCP4.5 and RCP8.5 atmospheric CO<sub>2</sub> trajectories through the 21<sup>st</sup> century with the well-  
107 tested GENIE Earth system model<sup>8</sup> that broadly captures these responses. Distributing 1kg m<sup>-2</sup>  
108 yr<sup>-1</sup> of pulverised silicates across 20 Mkm<sup>2</sup> of tropical weathering ‘hotspots’ lowers  
109 atmospheric CO<sub>2</sub> concentrations by ~40 ppm (basalt) or ~140 ppm (harzburgite) by year 2100  
110 in both the RCP4.5 and RCP8.5 climate change scenarios (Fig. 2a, b). Increasing the  
111 application rate to 5 kg m<sup>-2</sup> yr<sup>-1</sup> over the same 20 Mkm<sup>2</sup> ‘hotspot’ areas lowers the  
112 atmospheric CO<sub>2</sub> concentration further by 150–180 ppm under both RCPs (Fig. 2c, d), with  
113 an increasing effect at deeper soil mixing depths. For RCP4.5, atmospheric CO<sub>2</sub> by 2100 is  
114 reduced from 540 ppm to 390–350 ppm (basalt) or 350–250ppm (harzburgite), sufficient to  
115 play a major role in stabilizing climate and avoid seeding long-term amplifying climate  
116 feedbacks<sup>17</sup> (Fig. 2). For the business-as-usual RCP8.5 scenario, however, the lowest  
117 simulated CO<sub>2</sub> concentration by year 2100 in the high-end weathering scenario is still ~730  
118 ppm (basalt) or 690–560 ppm (harzburgite) (Fig. 2d). This suggests even massive  
119 intervention in Earth’s carbon cycle with basalt is unable to drive atmospheric CO<sub>2</sub> down  
120 close to the target of 350 ppm by 2100, an estimated requirement for restoring planetary  
121 energy balance and stabilizing climate<sup>17</sup>.

122 Future climate warming averted (WA) by engineering CO<sub>2</sub> removal through enhanced  
123 weathering is dependent on climate sensitivity and the actual atmospheric CO<sub>2</sub> concentration.  
124 Calculated end-of-century ‘warming averted’ figures for the enhanced weathering scenarios  
125 using GENIE, which has a low-to-medium climate sensitivity, are summarized in Table 1.  
126 For high application rates, WA ranges from 0.9–2.2°C for RCP4.5 and 0.7–1.6°C for RCP8.5  
127 (Table 1). At low application rates, corresponding ranges of WA are 0.2–0.7°C for both  
128 RCPs (Table 1). These numbers suggest that, theoretically at least, negative emissions from  
129 enhanced weathering could play a role alongside conventional mitigation reducing net CO<sub>2</sub>  
130 emissions in limiting future warming<sup>25</sup>.

131 Unmitigated future increases in atmospheric CO<sub>2</sub> will not only drive climate change but  
132 also ocean acidification, including reduced saturation of surface waters with respect to  
133 aragonite, threatening reef-building coral ecosystems<sup>11-14</sup>. Artificially enhanced tropical  
134 weathering increases land-to-ocean fluxes of alkalinity and dissolved inorganic carbon and  
135 raises freshwater pH to the upper range of tropical rivers (Supplementary Information). These  
136 fluxes, together with reduced atmospheric CO<sub>2</sub> (Fig. 2), tend to counter the negative impacts  
137 on ocean carbonate chemistry (Figs. 3 and 4). Our simulations driven by decreased CO<sub>2</sub> (Fig.  
138 2) and increased alkalinity fluxes show that additions of 1 kg m<sup>-2</sup> yr<sup>-1</sup> of harzburgite or basalt  
139 across the weathering ‘hotspots’ can mitigate future ocean acidification by an average of  
140 around 0.1 pH units (Fig. 3a, b). A higher silicate application rate (5 kg m<sup>-2</sup> yr<sup>-1</sup>) reverses  
141 future surface ocean acidification under RCP4.5, restoring global mean surface ocean pH to  
142 year 2000 levels or even pre-industrial levels by 2100 (Fig. 3c). Even for RCP8.5, 5 kg m<sup>-2</sup>  
143 yr<sup>-1</sup> reduces ocean acidification by approximately two-thirds by year 2100 (Fig. 3d)  
144 (Supplementary Information).

145 Coral reef health is linked to the ocean’s aragonite saturation state ( $\Omega_a$ ), which affects the  
146 rate at which corals can precipitate this crystalline mineral form of calcium carbonate and  
147 build skeletons<sup>13,14</sup>. Modern coral reefs generally occur where open ocean waters have a  
148 value of  $\Omega_a$  above a postulated<sup>14</sup> critical threshold of ~3.5. But under RCP4.5, and especially  
149 RCP8.5,  $\Omega_a$  at reef sites drops to <3.5 by 2100 (Fig. 4), potentially threatening them with  
150 extinction<sup>14</sup>. In simulations for RCP4.5 and RCP8.5, enhanced weathering with 1 kg m<sup>-2</sup> yr<sup>-1</sup>  
151 of silicates (basalt or harzburgite) and reduced atmospheric CO<sub>2</sub>, generates conditions of  $\Omega_a$   
152 >3.5 across main regions of coral reef occurrence (Fig. 4a–e). Hence, although this low  
153 dosage is rather ineffective at reducing global CO<sub>2</sub> (Fig. 2), it has specific regional advantages  
154 in terms of helping protect coral reefs. Applications of either rock at high rates (5 kg m<sup>-2</sup> yr<sup>-1</sup>)  
155 markedly increase  $\Omega_a$  above 3.5 in both RCP4.5 and RCP8.5 scenarios at low latitudes (Fig.  
156 4c,f). Enhanced weathering on land could therefore be more effective at alleviating stressors  
157 on coral reef health, including ocean acidification, than enhanced open-ocean dissolution of  
158 olivine<sup>26,27</sup>.

159 Our spatial and temporal analyses incorporate detailed plant-soil-climate interactions  
160 regulating soil mineral weathering rates. Driven by detailed geographical variations in  
161 projections of 21<sup>st</sup> century climate change and vegetation activity, they indicate the maximum  
162 potential of enhanced weathering for climate change mitigation, including amelioration of

163 ocean acidification. However, our scenarios represent a suite of idealized cases in which  
164 application of pulverised silicate rocks over forests is assumed to be achievable over large  
165 regions. Consequently, they help define the maximum potential CDR capacity of the  
166 approach. Not only will practical barriers to mineral transport and distribution on biodiverse  
167 tropical forests limit large-scale deployment, but roll-out on such a large-scale may be  
168 undesirable from both conservation and ecosystem services viewpoints. Deployment might  
169 be achievable in areas undergoing reforestation/afforestation or on agricultural lands where  
170 existing infrastructure could be utilized for rock grain distribution and management.  
171 However, well-documented field studies on graded spatial scales are needed prior to any  
172 significant implementation.

173 Large-scale geoengineering is ethically fraught<sup>15</sup> and poses dangers of both foreseeable  
174 and unforeseen consequences. Enhanced weathering employs naturally occurring minerals  
175 and reactions and therefore falls in the category of “soft geoengineering” along with  
176 reforestation, and agricultural techniques increasing soil carbon storage<sup>28</sup>. Nevertheless, it  
177 still requires comprehensive environmental impact assessments and dust mitigation strategies  
178 at production and deployment sites. Additionally, the production and distribution of  
179 pulverised rock carries health risks to anyone coming in contact with it because the particle  
180 sizes involved are respirable (Supplementary Information). Harzburgite, for example,  
181 includes asbestos-related minerals that carry health risks to local populations near application  
182 sites. However, carefully implemented, enhanced weathering may have added benefits,  
183 including fertilizing ocean and terrestrial CO<sub>2</sub> capture by marine diatoms<sup>3,26,29</sup> and tropical  
184 forests, respectively. Such effects, which are not considered here, could help offset energy  
185 costs<sup>3,5</sup> associated with extensive rock mining, grinding and transportation operations that  
186 might lower its sequestration capacity by ~8–33%.

187 Estimated implementation costs (combined capital and operational) for achieving an  
188 initial 50 ppm drawdown of atmospheric CO<sub>2</sub> are \$60–600 trillion for mining, grinding and  
189 transportation, assuming no technological innovation, with similar associated additional costs  
190 for distribution (Supplementary Information). On this basis, costs of enhanced weathering as  
191 a ‘negative emissions’ option exceed an estimate of \$50–200 trillion<sup>17</sup> for air capture of 50  
192 ppm CO<sub>2</sub>, but with the latter being less effective in reducing ocean acidification in important  
193 coral reef regions. These issues support calls for the alternative of a rising international  
194 carbon fee<sup>17</sup>. We proffer enhanced weathering not as a panacea for erasing impacts of fossil



195 fuel burning, but as a sobering indication of actions that may be required if fossil fuel  
196 emissions are not phased-down rapidly.

197 **Methods**

198 Methods and any associated references are available in the online version of the paper.

199

## 200 **References**

- 201 1 Seifritz, W. CO<sub>2</sub> disposal by means of silicates. *Nature* **345**, 486, doi:10.1038/345486b0  
202 (1990).
- 203 2 Schuiling, R. D. & Krijgsman, P. Enhanced weathering: An effective and cheap tool to  
204 sequester CO<sub>2</sub>. *Clim. Change* **74**, 349-354, doi:10.1007/s10584-005-3485-y (2006).
- 205 3 Köhler, P., Hartmann, J. & Wolf-Gladrow, D. A. Geoengineering potential of artificially  
206 enhanced silicate weathering of olivine. *Proc. Natl. Acad. Sci. U.S.A.* **107**, 20228-20233,  
207 doi:10.1073/pnas.1000545107 (2010).
- 208 4 Hartmann, J. *et al.* Enhanced chemical weathering as a geoengineering strategy to reduce  
209 atmospheric carbon dioxide, supply nutrients, and mitigate ocean acidification. *Rev.*  
210 *Geophys.* **51**, 113-149, doi:10.1002/rog.20004 (2013).
- 211 5 Moosdorf, N., Renforth, P. & Hartmann, J. Carbon dioxide efficiency of terrestrial  
212 enhanced weathering. *Environ. Sci. Technol.* **48**, 4809-4816, doi:10.1021/es4052022  
213 (2014).
- 214 6 Taylor, L. L., Banwart, S. A., Leake, J. R. & Beerling, D. J. Modeling the evolutionary  
215 rise of ectomycorrhiza on sub-surface weathering environments and the geochemical  
216 carbon cycle. *Am. J. Sci.* **311**, 369-403, doi:10.2475/05.2011.01 (2011).
- 217 7 Taylor, L. L., Banwart, S. A., Valdes, P. J., Leake, J. R. & Beerling, D. J. Evaluating the  
218 effects of terrestrial ecosystems, climate and carbon dioxide on weathering over  
219 geological time: a global-scale process-based approach. *Philos. Trans. R. Soc. B-Biol.*  
220 *Sci.* **367**, 565-582, doi:10.1098/rstb.2011.0251 (2012).
- 221 8 Cao, L. *et al.* The role of ocean transport in the uptake of anthropogenic CO<sub>2</sub>.  
222 *Biogeosciences* **6**, 375-390, doi:10.5194/bg-6-375-2009 (2009).
- 223 9 Hempel, S., Frieler, K., Warszawski, L., Schewe, J. & Piontek, F. A trend-preserving bias  
224 correction - the ISI-MIP approach. *Earth Syst. Dynam.* **4**, 219-236, doi:10.5194/esd-4-  
225 219-2013 (2013).
- 226 10 Taylor, K. E., Stouffer, R. J. & Meehl, G. A. An overview of CMIP5 and the experiment  
227 design. *Bull. Am. Met. Soc.* **93**, 485-498, doi:10.1175/BAMS-D-11-00094.1 (2011).
- 228 11 Caldeira, K. & Wickett, M. E. Anthropogenic carbon and ocean pH. *Nature* **425**, 365-  
229 365, doi:10.1038/425365a (2003).
- 230 12 Ciais, P. *et al.* in *Climate change 2013: The Physical Science Basis. Contribution of*  
231 *Working Group I to the Fifth Assessment Report of the Intergovernmental Panel on*

- 232 *Climate Change* (eds T. F. Stocker *et al.*) Ch. 6, 465-570 (Cambridge University Press,  
233 Cambridge, UK and New York, USA, 2013).
- 234 13 Turley, C. *et al.* The societal challenge of ocean acidification. *Marine Pollution Bull.* **60**,  
235 787-792, doi:10.1016/j.marpolbul.2010.05.006 (2010).
- 236 14 Rieke, K. L., Orr, J. C., Schneider, K. & Caldeira, K. Risks to coral reefs from ocean  
237 carbonate chemistry changes in recent earth system model projections. *Environ. Res.*  
238 *Lett.* **8**, 6, doi:10.1088/1748-9326/8/3/034003 (2013).
- 239 15 Caldeira, K., Bala, G. & Cao, L. The science of geoengineering. *Annu. Rev. Earth Planet.*  
240 *Sci.* **41**, 231-256, doi:10.1146/annurev-earth-042711-105548 (2013).
- 241 16 United Nations Framework Convention on Climate Change, available at  
242 <http://www.unfccc.int>. (1992).
- 243 17 Hansen, J. *et al.* Assessing “dangerous climate change”: required reduction of carbon  
244 emissions to protect young people, future generations and nature. *PLoS ONE* **8**, e81648,  
245 doi:10.1371/journal.pone.0081648 (2013).
- 246 18 Committee on Geoengineering Climate: Technical Evaluation and Discussion of Impacts;  
247 Board on Atmospheric Sciences and Climate; Ocean Studies Board; Division on Earth  
248 and Life Studies; National Research Council, Climate Intervention: Carbon Dioxide  
249 Removal and Reliable Sequestration, ISBN 978-0-309-30529-7. (National Academy of  
250 Sciences, Washington D. C., 2015).
- 251 19 Hartmann, J., Jansen, N., Dürr, H. H., Kempe, S. & Köhler, P. Global CO<sub>2</sub>-consumption  
252 by chemical weathering: What is the contribution of highly active weathering regions?  
253 *Global Planet. Change* **69**, 185-194, doi:10.1016/j.gloplacha.2009.07.007 (2009).
- 254 20 Wignall, P. B. Large igneous provinces and mass extinctions. *Earth-Sci. Rev.* **53**, 1-33,  
255 doi:10.1016/s0012-8252(00)00037-4 (2001).
- 256 21 Hilf, H. H. The manuring of poor soils with basalt grit. *Forstarchiv.* **14**, 93-101 (1938).
- 257 22 de Villiers, O. D. Soil rejuvenation with crushed basalt in Mauritius Part I: Consistent  
258 results of world-wide interests. *Int. Sugar J.* **63**, 363-364 (1961).
- 259 23 Anda, M., Shamshuddin, J. & Fauziah, C. I. Increasing negative charge and nutrient  
260 contents of a highly weathered soil using basalt and rice husk to promote cocoa growth  
261 under field conditions. *Soil Tillage Res.* **132**, 1-11, doi:10.1016/j.still.2013.04.005  
262 (2013).
- 263 24 Gillman, G. P., Burkett, D. C. & Coventry, R. J. Amending highly weathered soils with  
264 finely ground basalt rock. *Appl. Geochem.* **17**, 987-1001, doi:10.1016/S0883-  
265 2927(02)00078-1 (2002).

- 266 25 Gasser, T., Guivarch, C., Tachiiri, K., Jones, C. D. & Ciais, P. Negative emissions  
267 physically needed to keep global warming below 2 °C. *Nat Commun* **6**,  
268 doi:10.1038/ncomms8958 (2015).
- 269 26 Köhler, P., Abrams, J. F., Völker, C., Hauck, J. & Wolf-Gladrow, D. A. Geoengineering  
270 impact of open ocean dissolution of olivine on atmospheric CO<sub>2</sub>, surface ocean pH and  
271 marine biology. *Environ. Res. Lett.* **8**, 014009 (2013).
- 272 27 Hangx, S. J. T. & Spiers, C. J. Coastal spreading of olivine to control atmospheric CO<sub>2</sub>  
273 concentrations: A critical analysis of viability. *Int. J. Greenhouse Gas Control* **3**, 757-  
274 767, doi:10.1016/j.ijggc.2009.07.001 (2009).
- 275 28 Royal Society Report - Geoengineering the climate: science, governance and uncertainty.  
276 Report No. RS1636, (The Royal Society, London, 2009).
- 277 29 Bernard, C. Y., Dürr, H. H., Heinze, C., Segschneider, J. & Maier-Reimer, E.  
278 Contribution of riverine nutrients to the silicon biogeochemistry of the global ocean – a  
279 model study. *Biogeosciences* **8**, 551-564, doi:10.5194/bg-8-551-2011 (2011).

280 **Supplementary Information** is linked to the online version of the paper at [www.nature.com/nature](http://www.nature.com/nature)

281 **Acknowledgements** We thank Yves Godd ris and Phil Renforth for helpful comments on the  
282 manuscript, Tim Elliot for earlier discussions, and gratefully acknowledge funding through an ERC  
283 Advanced grant to D.J.B. (CDREG, 32998). We acknowledge the World Climate Research  
284 Programme's Working Group on Coupled Modelling, which is responsible for CMIP, and we thank  
285 the climate modelling groups (Table S1) for producing and making available their model output. For  
286 CMIP the U.S. Department of Energy's Program for Climate Model Diagnosis and Intercomparison  
287 provides coordinating support and led development of software infrastructure in partnership with the  
288 Global Organization for Earth System Science Portals.

289 **Author Contributions** D.J.B. conceived the study with input from all co-authors. L.L.T. undertook  
290 weathering model development and simulations, J.Q. and R.M.S.T. undertook data analyses, P.A.K.  
291 and A.R. provided model set-up support and advice, M.R.L. analysed the CMIP5 climates. D.J.B. led  
292 the writing with contributions from all co-authors, especially J.H., A.R., J.Q. and L.L.T.

293 **Author Information** Reprints and permissions information is available at [www.nature.com/reprints](http://www.nature.com/reprints).  
294 The authors declare no competing financial interests. Correspondence and requests for materials  
295 should be addressed to D.J.B. ([d.j.beerling@sheffield.ac.uk](mailto:d.j.beerling@sheffield.ac.uk)).

**Figure Legends**

297 **Figure 1. Enhanced weathering from pulverised silicate rock additions to the tropics**  
298 **increases CO<sub>2</sub> consumption.** End-of-century CO<sub>2</sub> consumption by enhanced terrestrial  
299 weathering with (a) dunite, (b) harzburgite or (c) basalt as a function of total rock applied,  
300 defined as the product of rate and an increasing treated land area in the tropics (30°S to 30°N).  
301 Simulations are shown for the Representative Concentration Pathway (RCP) 8.5; median and  
302 range for five climate model simulations for each application scenario. Symbols indicate  
303 reductions in CO<sub>2</sub> consumption and total rock applied when application is limited to 20 Mkm<sup>2</sup>  
304 of tropical weathering hotspots; symbol shape and fill denotes application rate and mixing  
305 depth scenario, respectively, for each curve. Vertical red lines show estimated total resources  
306 for each rock type (for basalt, solid, dashed and dot-dashed lines represent basalt resources in  
307 each of the Ethiopian, Deccan and Paraná Traps, respectively). The shaded area denotes  
308 uncertainty in upper values of global dunite resource availability (Supplementary  
309 Information). Panels (d) to (f) display the corresponding ensemble ranges for high and low  
310 application scenarios for each of five climate model simulations for both RCP8.5 and RCP4.5,  
311 assuming a mixing depth of 30 cm.

312 **Figure 2. Enhanced weathering lowers atmospheric CO<sub>2</sub> with projected 21<sup>st</sup> century**  
313 **climate change.** Effects of low additions (1 kg m<sup>-2</sup> yr<sup>-1</sup>) of silicate rock to 20 Mkm<sup>2</sup> of  
314 tropical weathering hotspots for two mixing depths (10 cm and 30 cm) on the atmospheric  
315 CO<sub>2</sub> concentration for (a) RCP4.5 (medium-level mitigation) and (b) RCP8.5 (business-as-  
316 usual). Panels (c) and (d) show comparable results for the effect of higher additions (5 kg m<sup>-2</sup>  
317 yr<sup>-1</sup>) of silicate rocks to the same areas of the tropics. In all panels, the pale blue line indicates  
318 the ‘control’ run with RCP-driven weathering, without additions of silicate rock. Envelopes  
319 and lines (solid 10 cm/dashed 30 cm) show the smoothed (five-year boxcar) ranges and  
320 medians, respectively, of results from five climate models for each RCP.

321 **Figure 3. Enhanced weathering ameliorates future ocean acidification caused by**  
322 **projected 21<sup>st</sup> century increases in atmospheric CO<sub>2</sub>.** Effects of increased alkalinity fluxes  
323 resulting from additions of 1 kg m<sup>-2</sup> yr<sup>-1</sup> of silicate rock to 20 Mkm<sup>2</sup> of tropical weathering  
324 hotspots mixed to two soil depths on global surface ocean pH for (a) RCP4.5 (medium-level  
325 mitigation) and (b) RCP8.5 (business-as-usual). Panels (c) and (d) show comparable results  
326 for the effect of higher additions (5 kg m<sup>-2</sup> yr<sup>-1</sup>) of silicate rocks to the tropics on global  
327 surface ocean pH for RCP4.5 and RCP8.5 respectively. Envelopes and lines (solid 10  
328 cm/dotted 30 cm mixing depths) show the smoothed (five-year boxcar) ranges and medians,  
329 respectively, of results from five climate models for each RCP.

330 **Figure 4. Enhanced weathering raises the aragonite saturation state of the ocean by**  
331 **2100.** Simulated global distribution of the aragonite saturation state ( $\Omega_a$ ) of the surface ocean  
332 in 2100 for RCP4.5 (a) no addition of silicate rocks, 1 kg m<sup>-2</sup> yr<sup>-1</sup> of (b) basalt and (c)  
333 harzburgite distributed over the tropics. Corresponding simulations for RCP8.5 are given in  
334 (d), (e) and (f) for applications of 5 kg m<sup>-2</sup> yr<sup>-1</sup>. Each panel displays in black the distribution  
335 of reef-building corals ([www.reefbase.org](http://www.reefbase.org)). All simulations are for a mixing depth of 30 cm.

## 336 **Methods**

337 **Terrestrial rock weathering modelling.** Terrestrial vegetation delivers the carbon-energy  
338 flux in the form of photosynthate to roots and associated mycorrhizal fungal networks which  
339 fuels biotic rates of mineral dissolution<sup>30</sup>. In our rock weathering model, the sub-surface  
340 organic carbon flux is stoichiometrically coupled to the rate of primary production and the  
341 uptake of inorganic nutrient ions by roots and mycorrhizal fungi which regulate the ionic  
342 composition and charge balance of the microscopic region of soil pore fluids at the organism-  
343 mineral interface (the mycorrhizosphere)<sup>6,7</sup>. This balance controls local pore fluid pH and  
344 organic ligand concentrations at the reacting mineral surfaces that control the rates of mineral  
345 dissolution through well-described reaction mechanisms<sup>31</sup>. We therefore couple an extended  
346 version of a previously published rock weathering model<sup>6,7</sup> with the Sheffield Dynamic  
347 Global Vegetation Model (SDGVM)<sup>32</sup>. Our simulations employed fixed land use patterns<sup>33</sup>.  
348 The SDGVM simulates terrestrial carbon, nitrogen and water cycling by vegetation and soils  
349 including land surface net primary productivity (NPP), hydrology, autotrophic and  
350 heterotrophic soil respiration, and dissolved organic carbon pools<sup>32</sup>. SDGVM is comparable  
351 in its sensitivity of response to CO<sub>2</sub> and climate to other DGVMs<sup>34,35</sup>.

352 In the extended weathering model, rainwater with an initial pH determined by the  
353 partial pressure and solubility of atmospheric CO<sub>2(g)</sub> and ion charge balance percolates  
354 through the soil at a rate determined by the SDGVM runoff. Soil solution chemistry is  
355 calculated both within and outside the mycorrhizosphere within the soil profile, which is  
356 divided into 10 layers specified at increasing depths, with runoff composition from each layer  
357 mixed and advected into the next layer. Mixing of bulk soil and mycorrhizosphere water is  
358 conceptualised as, but not explicitly parameterised as, hydrodynamic dispersion and diffusive  
359 exchange of bulk soil fluid solutes with the decreasing mycorrhizosphere volume with depth<sup>6</sup>,  
360 and pore fluid transport to plant roots for transpiration. The model recalculates the soil  
361 solution chemistry of each layer, with the dissolution reaction progress of primary silicate  
362 minerals ceasing upon reaching the theoretical saturation state of the fluid with respect to the  
363 dissolving mineral. Thermodynamic equilibria constrain both the forward reaction for  
364 mineral dissolution (see Eq. 1 below) and the concurrent precipitation of secondary phases  
365 including kaolinite, gibbsite and amorphous silica which act as sinks for dissolved Al and Si  
366 released by weathering. On carbonate-bearing lithologies, pore fluids are equilibrated with  
367 any calcite, dolomite or gypsum which might be present before weathering of any silicate

368 minerals present takes place. This treatment assumes sufficient carbonates to maintain  
 369 solubility equilibrium during the simulation time horizon and is not suitable for trace amounts  
 370 of carbonate minerals which would become completely depleted in non-carbonate lithologies.  
 371 Soil solution chemistry, therefore, depends on solubility equilibrium with existing carbonate  
 372 or sulphate minerals, precipitation of secondary phases, including kaolinite and amorphous  
 373 silica, and weathering of primary silicate minerals.

374 Underlying the weathering model is a rasterised version of the Hartmann & Moosdorf<sup>36</sup>  
 375 lithological map for which we prepared a lithological database giving the proportions of the  
 376 parent minerals in each rock type. Each rock type has its own mineral assemblage (see  
 377 below), and each mineral  $m$  weathers according to the general rate law<sup>37</sup> with mineral-  
 378 specific parameter values for  $SA$ ,  $k$ ,  $n$  and  $E$ :

$$379 \quad Rate_m = SA_m \sum_i \left[ k_{i,m}^{298.15} \exp \left[ \frac{-E_{i,m}}{R} \left( \frac{1}{T} - \frac{1}{298.15} \right) \right] a_i^{n_{i,m}} \left( 1 - \left[ \frac{Q_m}{K_{sp,m}} \right] \right) \right] \quad \text{Eq. (1)}$$

380 where  $Rate_m$  is given in mol m<sup>-2</sup> mineral s<sup>-1</sup>,  $SA$  is mineral surface area (m<sup>2</sup>),  $i$  is the individual  
 381 weathering agent, such as [H<sup>+</sup>],  $k_{i,m}$  is the rate constant,  $E_{i,m}$  is the apparent activation energy  
 382 (kJ mol<sup>-1</sup>),  $R$  is the gas constant (kJ mol<sup>-1</sup> K<sup>-1</sup>),  $T$  is temperature (K),  $a_i$  is the molar activity of  
 383 weathering agent  $i$  (mol l<sup>-1</sup>) and  $n_{i,m}$  is the reaction order.  $Q_m = \prod_j a_j^{s_j}$  is the ion activity  
 384 product of the soil solution, where  $a_j$  is the activity of solute  $j$  raised to the power of its  
 385 stoichiometry  $s_j$  on the product side of the chemical equation describing the dissolution of  
 386 mineral  $m$  (Tables S2, S3).  $K_{sp,m}$  is the solubility constant for mineral  $m$  (Table S2).  
 387 Activities are approximated by concentrations.

388 The model accounts for changes in mineral surface area due to relief (standard deviation  
 389 of orography) as described previously<sup>7</sup> and includes an empirical surface area correction for  
 390 each rock type which accounts for age effects<sup>38</sup>, internal porosity, grain size errors and  
 391 deviation of particle shape from perfect spheres. Soil water residence times and riverine  
 392 fluxes depend on run-off calculated by SDGVM. The model calculates monthly fluxes of  
 393 CO<sub>2</sub> consumption, alkalinity (Ca<sup>2+</sup>, Mg<sup>2+</sup>, K<sup>+</sup> and Na<sup>+</sup>) and dissolved inorganic carbon and is  
 394 verified against water chemistry and discharge data from a global suite of river catchments

395 **Validation.** Simulated terrestrial fluxes of CO<sub>2</sub> consumed by rock weathering in 42  
 396 watersheds worldwide<sup>39</sup> using the CRU-3 climate<sup>40</sup> at 1° × 1° resolution are validated against  
 397 fluxes derived from catchment-scale estimates based on stream-water chemistry



398 (Supplementary Information). We generated fluxes for basins in the World Resources  
399 Institute's shapefile<sup>41</sup> and compared these to the 45 basins (Table 3 in Ref. 39) where the  
400 basin names could be matched. Given the test aims to compare model and observed  
401 weathering rates, three catchments were rejected on the basis of markedly different basin  
402 areas or runoff (defined as two standard deviations of the mean residual). Therefore, 42  
403 basins were retained for validation, except in the case of carbonate CO<sub>2</sub> consumption, where  
404 an additional five basins were excluded due to lack of carbonates in the modelled lithologies.

405 The response of modelled weathering rates in Iceland to temperature change accords with  
406 observed chemical weathering flux responses to climate warming over the past four decades  
407 in un-glaciated Icelandic catchments<sup>42</sup>. Regional responses also support the CO<sub>2</sub> and climate  
408 change sensitivity of our approach. Adopting a more complex soil weathering module  
409 coupled to a DGVM<sup>43</sup>, another group predicted a similar increase in CO<sub>2</sub> consumption in the  
410 Mackenzie River arctic watershed from 355 ppm CO<sub>2</sub> and modern climate to 560 ppm CO<sub>2</sub>  
411 with an associated warmer climate, based on results from the RCP4.5 simulations  
412 (Supplementary Information). Estimated pH values of river run-off calculated from alkalinity  
413 fluxes and equilibrated to ambient CO<sub>2</sub>, are comparable to measurements reported for a range  
414 of tropical river catchments (Supplementary Information).

415 **Geoengineering simulations.** For the atmospheric CO<sub>2</sub> concentration trajectories defined by  
416 the two RCPs considered here (RCP4.5 and RCP8.5), the five General Circulation Models  
417 (GCMs) produce monthly temperature, relative humidity and precipitation to drive SDGVM.  
418 Monthly climate datapoints closest to the desired coordinates are bilinearly interpolated in  
419 space before daily values for the month are estimated using climate statistics. These  
420 estimated daily climates force SDGVM. Distributed silicate rock grains are treated as perfect  
421 monomineralogical spheres with a nominal starting diameter of 10 μm. Initial total surface  
422 areas for the added silicates are calculated for each mineral using the total mass applied,  
423 specified diameter, weight fraction for the mineral, mineral specific gravity and the equations  
424 for the volume and surface area of a sphere. As weathering progresses, mass is removed and  
425 the fractional change in total surface area is estimated using the fractional change in mass  
426 raised to the power  $\frac{2}{3}$ . This treatment assumes that each particle is a shrinking sphere. The  
427 total mass and surface area for each mineral are increased according to dose rate. No attempt  
428 is made to model a particle size distribution for either the starting silicate rock grain size or  
429 the individual mineral residues following weathering. Pulverized silicates are mixed with a

430 specified depth of soil, without modelling bioturbation processes or the transport behaviour of  
431 suspended materials in infiltrating water. Soil water residence times and riverine fluxes  
432 depend on runoff modelled by SDGVM. Mean reactive surface areas of autochthonous  
433 primary soil minerals are corrected for erosion and relief<sup>7</sup>. The model assumes no change in  
434 porosity or water movement with depth, and there is no preferential transport of different  
435 particle sizes.

436 **Mineralogy of pulverized silicates.** The mineralogy of each simulated pulverized silicate  
437 rock is listed in Table S4. The model basalt silicate mineralogy is based on the normative  
438 composition for a normal alkali tholeiitic basalt<sup>44</sup>, neglecting some minor phases such as  
439 magnetite. Our dunite composition follows Kogel *et al.*<sup>45</sup>. We use the mineralogy of the  
440 Troodos harzburgite, with lizardite rather than chrysotile (asbestos) as this is the dominant  
441 serpentine near Troodos<sup>46</sup> and as it is sensible to avoid rocks with a large proportion of  
442 asbestos for health reasons. Our results are therefore conservative with respect to the  
443 proportion of unserpentinised olivine and the relative amounts of lizardite and chrysotile  
444 present.

445 **GENIE Earth system global CO<sub>2</sub> and ocean biogeochemistry modelling.** The climate and  
446 ocean circulation of the GENIE Earth system model has been calibrated by 2-D reanalysis  
447 fields of surface air temperature and humidity and 3-D observational fields of ocean  
448 distributions of temperature and salinity<sup>47</sup>. The carbon cycle is calibrated against observed  
449 ocean phosphate and alkalinity distributions<sup>47,48</sup>. The resulting marine carbon cycle has been  
450 extensively used and evaluated, including against observations of natural (e.g.  $\Delta^{14}\text{C}$ ) and  
451 perturbed anthropogenic carbon cycling. GENIE is also compatible with observational  
452 uncertainty<sup>8</sup> and other (generally higher resolution) carbon cycle model responses to CO<sub>2</sub>  
453 perturbation<sup>49-51</sup>. The version used here is as summarized by Cao *et al.*<sup>8</sup> that includes a 76 m  
454 deep surface ocean and the cycling of Fe described by Annan and Hargreaves<sup>52</sup> (except with  
455 biological uptake following Doney *et al.*<sup>53</sup>), but lacks a mixed layer scheme. Our results  
456 therefore represent a pessimistic case for weathering and in the real world one might have a  
457 slightly shallower surface layer with even higher saturation. The addition of Fe co-limitation  
458 of marine biological export results in a <1% change in the projected year 1994 anthropogenic  
459 CO<sub>2</sub> inventory compared to the PO<sub>4</sub>-only model<sup>8</sup>.

460 We simulated the effects of CO<sub>2</sub> consumption by enhanced weathering on atmospheric  
461 CO<sub>2</sub> drawdown and ocean biogeochemistry in two steps. First, we diagnosed the annual CO<sub>2</sub>

462 emissions compatible with a particular RCP CO<sub>2</sub> concentration projection over the 21<sup>st</sup>  
463 century by prescribing that CO<sub>2</sub> curve and backing-out emissions. Cross-checking these  
464 diagnoses by performing forward simulations with annual CO<sub>2</sub> emissions in the absence of  
465 enhanced weathering reproduced the RCP4.5 and RCP8.5 CO<sub>2</sub> curves to within 1 ppm. Then,  
466 for each application scenario, we subtracted the annual CO<sub>2</sub> consumption due to enhanced  
467 weathering from the diagnosed RCP emissions and forced GENIE with the remainder.

468 The ocean biogeochemistry simulations incorporate reduced atmospheric CO<sub>2</sub> and  
469 increases in the alkalinity and dissolved inorganic carbon fluxes. In each case, those for  
470 2005–2015 and 2089–2099 are transferred to a 36 × 36 global grid, migrating land fluxes on  
471 the weathering model continents to the ocean following standard directional paths. GENIE  
472 linearly interpolated these flux forcings for intermediate years. All GENIE runs were based  
473 on the same starting state, comprising a 10,000-year pre-industrial spin-up followed by a  
474 transient experiment forced by historical changes in atmospheric CO<sub>2</sub> concentration up until  
475 year 2006 as described in Cao *et al.*<sup>8</sup> and Ridgwell *et al.*<sup>48</sup>.

476

477 30 Quirk, J., Andrews, M. Y., Leake, J. R., Banwart, S. A. & Beerling, D. J.

478 Ectomycorrhizal fungi and past high CO<sub>2</sub> atmospheres enhance mineral weathering  
479 through increased below-ground carbon-energy fluxes. *Biol. Lett.* **10**,  
480 doi:10.1098/rsbl.2014.0375 (2014).

481 31 Brantley, S. L. in *Kinetics of Water-Rock Interaction* (eds Susan L. Brantley, James D.  
482 Kubicki, & F. Art White) Ch. 5, 151-210 (Springer, 2008).

483 32 Woodward, F. I. & Lomas, M. R. Vegetation dynamics - simulating responses to climatic  
484 change. *Biol. Rev.* **79**, 643-670, doi:10.1017/s1464793103006419 (2004).

485 33 Bartholomé, E. & Belward, A. S. GLC2000: a new approach to global land cover  
486 mapping from Earth observation data. *Int. J. Remote Sens.* **26**, 1959-1977,  
487 doi:10.1080/01431160412331291297 (2005).

488 34 Friend, A. D. *et al.* Carbon residence time dominates uncertainty in terrestrial vegetation  
489 responses to future climate and atmospheric CO<sub>2</sub>. *Proc. Natl. Acad. Sci. U.S.A.* **111**,  
490 3280-3285, doi:10.1073/pnas.1222477110 (2014).

491 35 Sitch, S. *et al.* Evaluation of the terrestrial carbon cycle, future plant geography and  
492 climate-carbon cycle feedbacks using five Dynamic Global Vegetation Models

- 493 (DGVMS). *Glob. Change Biol.* **14**, 2015-2039, doi:10.1111/j.1365-2486.2008.01626.x  
494 (2008).
- 495 36 Hartmann, J. & Moosdorf, N. The new global lithological map database GLiM: A  
496 representation of rock properties at the Earth surface. *Geochem. Geophys. Geosys.* **13**,  
497 doi:10.1029/2012gc004370 (2012).
- 498 37 Palandri, J. L. & Kharaka, Y. K. A compilation of rate parameters of water-mineral  
499 interaction kinetics for application to geochemical modeling. Report No. 2004-1068, 1-  
500 64 (U.S. Geological Survey, Menlo Park, California, 2004).
- 501 38 White, A. F. & Brantley, S. L. The effect of time on the weathering of silicate minerals:  
502 why do weathering rates differ in the laboratory and field? *Chem. Geol.* **202**, 479-506,  
503 doi:10.1016/j.chemgeo.2003.03.001 (2003).
- 504 39 Gaillardet, J., Dupré, B., Louvat, P. & Allègre, C. J. Global silicate weathering and CO<sub>2</sub>  
505 consumption rates deduced from the chemistry of large rivers. *Chem. Geol.* **159**, 3-30,  
506 doi:10.1016/S0009-2541(99)00031-5 (1999).
- 507 40 Mitchell, T. D. & Jones, P. D. An improved method of constructing a database of  
508 monthly climate observations and associated high-resolution grids. *Int. J. Climatology*  
509 **25**, 693-712, doi:10.1002/joc.1181 (2005).
- 510 41 Food Agriculture Organization of the United Nations. FAO GEONETWORK. (FAO,  
511 Rome, Italy, 2014).
- 512 42 Gislason, S. R. *et al.* Direct evidence of the feedback between climate and weathering.  
513 *Earth. Planet. Sci. Lett.* **277**, 213-222, doi:10.1016/j.epsl.2008.10.018 (2009).
- 514 43 Beaulieu, E., Godderis, Y., Donnadieu, Y., Labat, D. & Roelandt, C. High sensitivity of  
515 the continental-weathering carbon dioxide sink to future climate change. *Nature Clim.*  
516 *Change* **2**, 346-349, doi:10.1038/nclimate1419 (2012).
- 517 44 Nockolds, S. R. Average chemical compositions of some igneous rocks. *Geol. Soc. Am.*  
518 *Bull.* **65**, 1007-&, doi:10.1130/0016-7606(1954)65[1007:accosi]2.0.co;2 (1954).
- 519 45 Kogel, J. E., Trivedi, N. C., Barker, J. M. & Krukowski, S. T. *Industrial minerals and*  
520 *rocks - commodities, markets, and uses*. 7th edn, (Society for Mining, Metallurgy, and  
521 Exploration, 2006).
- 522 46 Magaritz, M. & Taylor, H. P. Oxygen and hydrogen isotope studies of serpentinization in  
523 Troodos ophiolite complex, Cyprus. *Earth. Planet. Sci. Lett.* **23**, 8-14, doi:10.1016/0012-  
524 821x(74)90023-5 (1974).

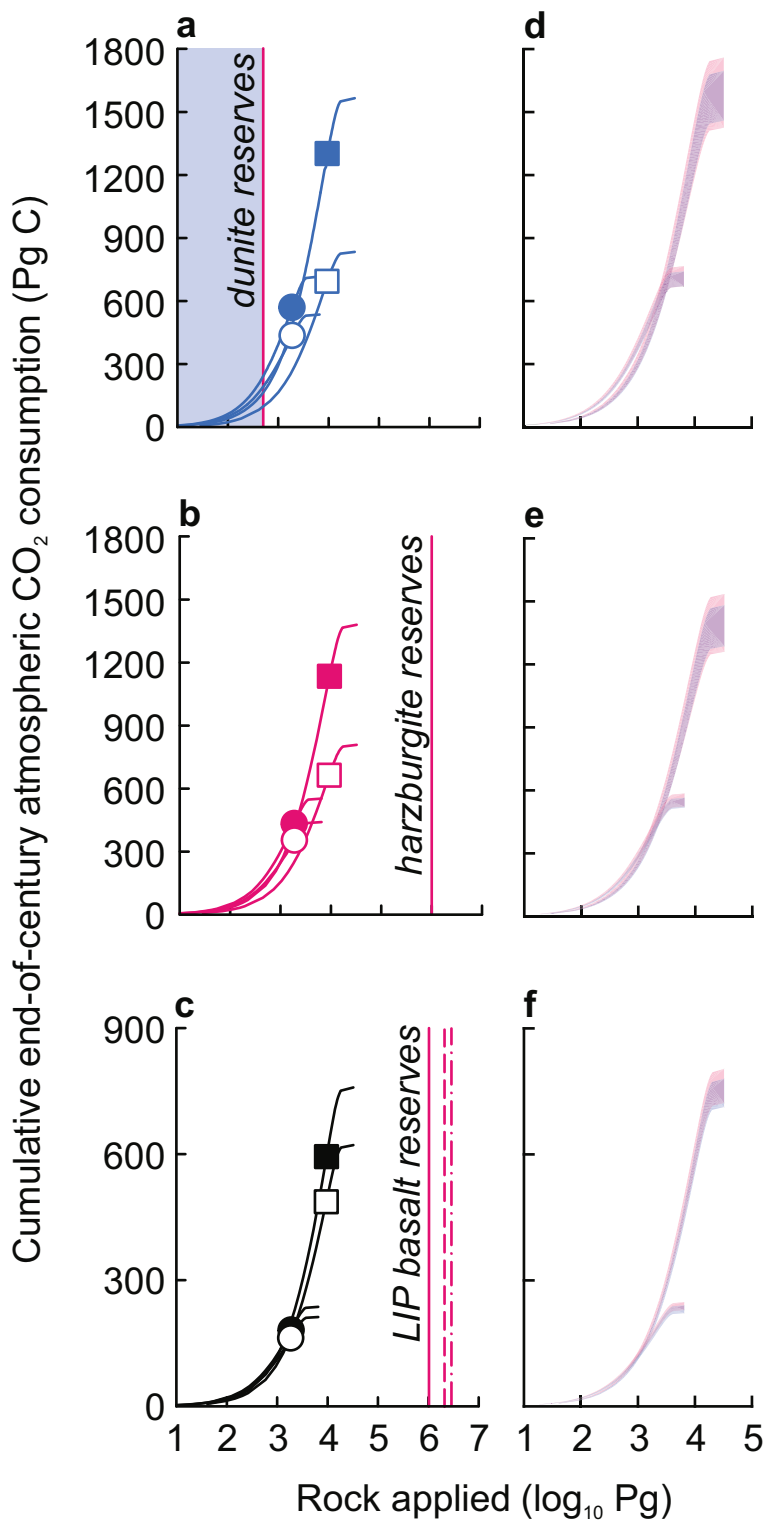
- 525 47 Price, A. R., Myerscough, R. J., Voutchkov, I. I., Marsh, R. & Cox, S. J. Multi-objective  
526 optimization of GENIE Earth system models. *Philos. Trans. R. Soc. A-Math., Phys., &*  
527 *Engineer. Sci.* **367**, 2623-2633, doi:10.1098/rsta.2009.0039 (2009).
- 528 48 Ridgwell, A. *et al.* Marine geochemical data assimilation in an efficient Earth System  
529 Model of global biogeochemical cycling. *Biogeosciences* **4**, 87-104, doi:10.5194/bg-4-  
530 87-2007 (2007).
- 531 49 Archer, D. *et al.* Atmospheric lifetime of fossil fuel carbon dioxide. *Annu. Rev. Earth*  
532 *Planet. Sci.* **37**, 117-134, doi:10.1146/annurev.earth.031208.100206 (2009).
- 533 50 Eby, M. *et al.* Historical and idealized climate model experiments: an intercomparison of  
534 Earth system models of intermediate complexity. *Clim. Past* **9**, 1111-1140,  
535 doi:10.5194/cp-9-1111-2013 (2013).
- 536 51 Goodwin, P., Williams, R. G., Ridgwell, A. & Follows, M. J. Climate sensitivity to the  
537 carbon cycle modulated by past and future changes in ocean chemistry. *Nature Geosci.* **2**,  
538 145-150, doi:10.1038/ngeo416 (2009).
- 539 52 Annan, J. D. & Hargreaves, J. C. Efficient identification of ocean thermodynamics in a  
540 physical/biogeochemical ocean model with an iterative Importance Sampling method.  
541 *Ocean Model.* **32**, 205-215, doi:10.1016/j.ocemod.2010.02.003 (2010).
- 542 53 Doney, S. C., Lindsay, K., Fung, I. & John, J. Natural variability in a stable, 1000-yr  
543 global coupled climate-carbon cycle simulation. *J. Clim.* **19**, 3033-3054,  
544 doi:10.1175/JCLI3783.1 (2006).

545

**Table 1. Projected mean global air temperature and change in temperature at year 2100.** Values show mean  $\pm$  S.D. of five climate models (CMIP5) for the change in end-of-century mean global temperature simulated with the GENIE Earth system model using revised CO<sub>2</sub> trajectories associated with each rock type and application rate with an applied rock mixing depth of 30 cm (Figure 2).

	Warming at 2100 (°C)		Warming averted at 2100 (°C) <sup>a</sup>	
	RCP 4.5	RCP 8.5	RCP 4.5	RCP 8.5
Control (no enhanced weathering) <sup>b</sup>	1.4 $\pm$ 0.01	3.0 $\pm$ 0.01	n/a	n/a
IPCC range of projected warming <sup>c</sup> [Ref.12]	1.1 – 2.6	2.6 – 4.8	n/a	n/a
<i>Enhanced weathering scenario</i>				
Harzburgite (1 kg m <sup>-2</sup> yr <sup>-1</sup> )	0.8 $\pm$ 0.04	2.5 $\pm$ 0.04	0.7 $\pm$ 0.04	0.5 $\pm$ 0.04
Harzburgite (5 kg m <sup>-2</sup> yr <sup>-1</sup> )	-0.77 $\pm$ 0.2	1.4 $\pm$ 0.1	2.2 $\pm$ 0.2	1.6 $\pm$ 0.1
Basalt (1 kg m <sup>-2</sup> yr <sup>-1</sup> )	1.21 $\pm$ 0.02	2.8 $\pm$ 0.01	0.2 $\pm$ 0.02	0.2 $\pm$ 0.01
Basalt (5 kg m <sup>-2</sup> yr <sup>-1</sup> )	0.5 $\pm$ 0.05	2.25 $\pm$ 0.05	0.9 $\pm$ 0.05	0.7 $\pm$ 0.05

<sup>a</sup>Relative to control (no enhanced weathering); <sup>b</sup>Relative to 2005; <sup>c</sup>Relative to 1986 – 2005



**Application rate:**  
 squares 5 kg m<sup>-2</sup> yr<sup>-1</sup>  
 circles 1 kg m<sup>-2</sup> yr<sup>-1</sup>

**Mixing depth:**  
 filled 30 cm  
 open 10 cm

**RCP:**  
 purple 4.5  
 pink 8.5

